Control Engineering Practice 175 (2026) 107097

Contents lists available at ScienceDirect

Control Engineering Practice

journal homepage: www.elsevier.com/locate/conengprac

Capacity estimation of lithium-ion batteries using invariance property in open circuit voltage relationship

Yang Wang *, Marta Zagorowska, Riccardo M.G. Ferrari

Delft Center for Systems and Control, Delft University of Technology, Mekelweg 5, Delft, 2628, CD, Netherlands

ARTICLE INFO

Keywords:
Lithium-ion battery
Electric vehicles
Capacity estimation
Open circuit voltage

ABSTRACT

Lithium-ion (Li-ion) batteries are ubiquitous in electric vehicles (EVs) as efficient energy storage devices. The reliable operation of Li-ion batteries depends critically on the accurate estimation of battery capacity. However, conventional estimation methods require extensive training datasets from costly battery tests for modeling, and a full cycle of charge and discharge is often needed to estimate the capacity. To overcome these limitations, a capacity estimation method is proposed that leverages only one cycle of the open-circuit voltage (OCV) test in modeling and allows for estimating the capacity from partial charge or discharge data. Moreover, by applying it with OCV identification algorithms, the capacity can be estimated from dynamic discharge data without requiring dedicated data collection tests. The proposed method exploits an invariance property observed in the OCV versus state of charge relationship across aging cycles. Leveraging this invariance, the proposed method estimates the capacity by solving an OCV alignment problem using only the OCV and the discharge capacity data from the battery. Simulation results demonstrate the method's efficacy, achieving a mean absolute relative error of less than 0.4% with OCV test data and less than 2.6% with dynamic data in capacities across 10 aging batteries.

1. Introduction

Electric vehicles (EVs) are gaining increasing popularity in modern transportation due to their roles in reducing greenhouse gas emissions, leading to carbon neutralization (Hannan et al., 2017; Meng et al., 2018). Lithium-ion (Li-ion) batteries are renowned for their favorable energy density, energy efficiency, and extended service life, and are widely adopted in EVs as energy storage devices (Plett, 2015). As batteries undergo cycles of charge and discharge, they inevitably experience performance impairment, in which battery capacity declines significantly (Peng et al., 2025). This degradation deteriorates the performance of the EV's range and raises safety concerns. As a result, accurate monitoring of the battery capacity is crucial for reliable vehicle operation (Zhang et al., 2025).

Estimating the capacity of the battery primarily relies on three categories of approaches: direct measurement methods, model-based methods, and data-driven methods (Wang et al., 2023). Direct measurement approaches estimate battery capacity by applying Coulomb counting over a full charge or discharge cycle (Navidi et al., 2024). This method is straightforward, but it is inconvenient for EVs under operation as the battery is seldom in a fully discharged state, which can permanently damage the battery. Model-based methods enable online estimation of capacity from operational data using established battery models. Common models encompass empirical models and physical models. Empirical model-based approaches collect historical records of the capacity and operating conditions, e.g., the number of cycles, C-rate, and SOC span, and fit an empirical model to the data to relate these characteristics with capacity fade (Wan et al., 2025; Zagorowska et al., 2020). Physical model-based methods utilize an electrochemical model (EM) or an equivalent circuit model (ECM) to identify the capacity of the battery. The single particle model (SPM), a commonly used EM, relates microscopic degradation factors, e.g., the mass of active materials and the inventory of lithium-ions, to the battery capacity and simulates the capacity trajectory by modeling the trend of their degradation with the stress factors (El-Dalahmeh et al., 2023). The ECM correlates electrical parameters, e.g., internal resistance, open-circuit voltage (OCV), with battery capacity using data from aging tests. Then, it estimates the capacity during operation by identifying the current values of these parameters from operational data (Li et al., 2024). However, the practical application of EMs is hindered by the difficulty of accessing battery-specific chemical parameters and the requirement for substantial computational power. The ECM needs extensive experiments to establish an accurate correlation between battery parameters and degradation. These factors limit the application of model-based approaches in practical usage.

Data-driven methods are divided into feature-based methods and end-to-end methods. Feature-based methods establish machine

* Corresponding author.
E-mail addresses: y.wang-40@tudelft.nl (Y. Wang), m.a.zagorowska@tudelft.nl (M. Zagorowska), r.ferrari@tudelft.nl (R.M.G. Ferrari).

https://doi.org/10.1016/j.conengprac.2026.107097
Received 1 November 2025; Received in revised form 30 May 2026; Accepted 31 May 2026
Available online 6 June 2026

learning models that relate features from the OCV curve, such as the curve in differential voltage analysis (DVA) and incremental capacity analysis (ICA), to the capacity of the battery (Bloom et al., 2005; Navidi et al., 2024). End-to-end-based methods directly process measurement data, e.g., current, voltage, and temperature from battery operation, and infer from usage records the capacity of the battery using neural network architectures (Lianpo et al., 2025; Lu et al., 2022). Although showing promising results, data-driven approaches rely on extensive training data, the acquisition of which is costly and time- and energy-consuming.

A mechanistic model-based capacity estimation was proposed, leveraging the open circuit potential (OCP) of electrodes (Dubarry et al., 2012). The OCV of the full battery is obtained as the difference between the positive and the negative electrode potential. The degradations of active materials of the two electrodes and the loss of lithium-ion inventory are modeled as scaling and translation of the OCP curves, and the degradation of electrode capacity is estimated by fitting alignment parameters of the OCPs to the measured OCV (Schmitt et al., 2023). However, this approach requires the data of the half-cell OCP relationships, which rely on invasive experiments that open the battery and build a half-cell from samples of the electrodes. This type of experiment is repeated for each battery configuration, which is costly and induces safety concerns.

In this work, a capacity estimation method is proposed that leverages a geometric property in the OCV-SOC relationship. The method requires only one cycle of the OCV measurements from the nominal battery, eliminating the need for cumbersome OCV-SOC measurements across all aging cycles and the disassembling of the battery to build half-cell samples. With the OCV and discharge capacity data of the aged battery, the capacity is estimated throughout the battery's lifespan with sufficient accuracy. With an OCV estimation algorithm, this approach enables us to estimate the capacity from dynamic discharge data, without using additional capacity diagnostic tests, showing potential for online estimation of capacity from dynamic operational data.

The remainder of this paper is structured as follows. Section 2 introduces the concept of calibrated SOC and the developed capacity estimation method, Section 3 presents the estimation results on real-life battery data, Section 4 discusses the validity of the approach, and Section 5 presents concluding remarks of this study.

2. Battery capacity estimation

In this section, the concept of calibrated state of charge for aged batteries is first introduced, then the invariance property observed in the battery's open circuit voltage and state of charge (OCV-SOC) relationship is demonstrated, and finally, a capacity estimation method is proposed utilizing this invariance.

2.1. State of charge of aged batteries

The state of charge (SOC) is a critical component closely related to the capacity of the battery. It is the ratio of the charge stored in the cell to its total capacity. The correctness of SOC with respect to the true value of the battery is critically dependent on the capacity with which the SOC is computed. For an aged battery with a total capacity of 8 Ah and a nominal capacity of 10 Ah, when the battery is fully discharged, the SOC computed with 10 Ah is 20% while the actual SOC is 0%. This discrepancy in SOC can be used to estimate capacity with an invariance property in the shape of the OCV-SOC relationship.

To distinguish different ways of computing SOC, notations a and n are used to denote the aged and the nominal battery. $C_i \in \mathbb{R}_{>0}$ is defined as the capacity of the battery and $i \in \{a, n\}$ denotes the type of the battery, e.g., C_a is the aged capacity and C_n is the nominal capacity.

The discharge capacity is defined as the amount of charge withdrawn from the battery, and it is computed via Coulomb counting as:

$$Q^i_{dc}(t) = -\frac{1}{3600}\int_{t_0}^{t} I_b(\tau)d\tau, \tag{1}$$

where $Q^i_{dc}(t) \in \mathbb{R}$ is the discharge capacity for battery i, $i \in \{a, n\}$ in Ampere-hour (Ah), $I_b(t) \in \mathbb{R}$ is the load current of the battery (positive for charging), and 3600 is the factor converting Coulombs into Ah. t_0 is the initial time from which Q^i_{dc} starts being recorded for capacity estimation, and the initial discharge capacity $Q^i_{dc}(t_0)$ is defined as zero independent of the initial value of SOC. The SOC can be computed from $Q^i_{dc}(t)$ and the battery's total capacity C_j as:

$$Z^i_j(t) = Z^i_j(t_0) - \frac{Q^i_{dc}(t)}{C_j} \times 100\% \tag{2}$$

where $Z^i_j(t) \in [0, 1]$ is the SOC of battery i computed with the capacity C_j, $i, j \in \{a, n\}$, at time t, $Z^i_j(t_0) \in [0, 1]$ is the initial SOC, and $C_j \in \mathbb{R}_{>0}$ is the total capacity of the battery j in Ah.

When the type of the battery actually being discharged and the type of capacity used to compute the SOC are consistent, i.e., $i = j$, the SOC $Z^i_j(t)$ is defined as calibrated, i.e., $Z^a_a(t)$ and $Z^n_n(t)$ are calibrated SOCs, and the capacity is defined as the calibrated capacity, i.e., C_i is calibrated for battery i. When $i \neq j$, e.g., $Z^a_n(t)$, the SOC $Z^i_j(t)$ is uncalibrated, and the capacity is an uncalibrated capacity for battery i. Only the calibrated SOC can reflect the real state of the battery currently being operated[1].

The open circuit voltage (OCV) is the terminal voltage of the battery when it is disconnected from external circuits and rested for a sufficient amount of time. The OCV varies with SOC, and it will be shown that, when the SOC is calibrated, the OCV-SOC relationship is practically invariant across aging cycles. The OCV can be obtained using OCV identification algorithms from dynamic discharge data (Wang & Ferrari, 2025). The OCV and SOC are independently collected from the battery with a one-to-one mapping and are treated as a high-resolution lookup table used for capacity estimation. The OCV of the ith battery is denoted by $V^i_{oc}(t) \in \mathbb{R}$, $i \in \{a, n\}$, and the OCV-SOC relationship is denoted by $V_{oc}(Z(t))$, $Z(t) \in [\check{Z}, \hat{Z}]$. $\check{Z} \in \mathbb{R}$ and $\hat{Z} \in \mathbb{R}$, $\check{Z} \leq \hat{Z}$ are the upper and lower bounds of the SOC. The estimation of V_{oc} at any SOC point $Z(t) \in [\check{Z}, \hat{Z}]$ can be achieved through linear interpolation.

2.2. Invariance in OCV-SOC relationships

The OCV-SOC relationship can reveal the aging status of the battery. When the battery undergoes continuous aging, the total capacity of the battery decreases, and the OCV reaches the lower cut-off voltage sooner with less discharge capacity extracted from the battery. This behavior is illustrated in Fig. 1a and b. However, when the calibrated SOC is computed with the calibrated capacity, examination of the OCV-SOC relationships shows that the curves of the relationships are highly invariant across all degrees of aging of the battery.

This phenomenon is observed in batteries with different types of chemistries from different datasets. For example, Fig. 1a and b show the OCV versus discharge capacity relationships and the OCV-SOC relationships of a LiNiMnCoO2 (NMC) battery from the Stanford Aging dataset (Pozzato et al., 2022). Fig. 1a shows that the maximum discharge capacity at lower cut-off voltage decreases as the battery undergoes more and more aging cycles, and when the OCV is related to the calibrated SOC computed with the calibrated capacity, it can be seen from Fig. 1b that the OCV-SOC curves align closely with each other across aging cycles. The mean of RMSEs of the OCV-SOC relationships compared to the OCV-SOC curve of the nominal battery is 0.0132 V, only 0.31% of the upper cut-off voltage of the battery. A similar observation can be made from a LiMO2 (LMO) battery using the data from the Oxford Battery Degradation Dataset (Howey & Birkl, 2017) shown in Fig. 1c and d. The alignment of OCV-SOC relationships after calculating the calibrated SOC with the calibrated capacity is noticeably close, and the mean RMSE of the OCV curves is 0.0274 V, which is 0.65% of the battery's upper cut-off voltage.

[1] Note that $Z^n_a(t)$ can be defined with the above notation, but does not have a physical meaning and is unused in the paper

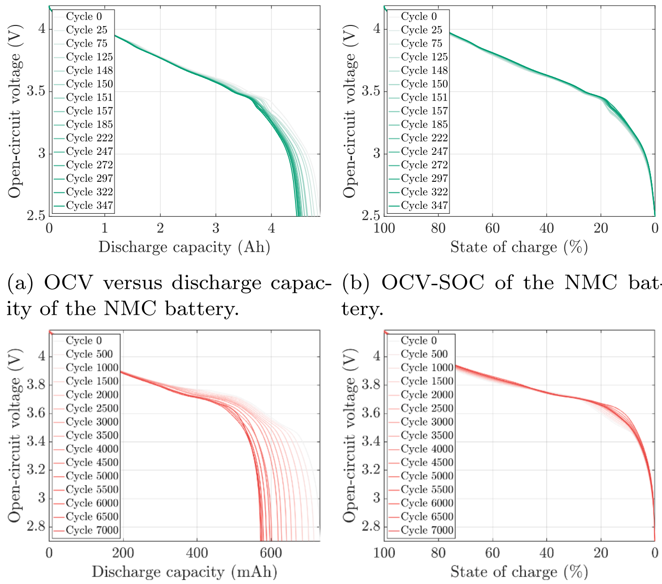

(a) OCV versus discharge capacity of the NMC battery.

(b) OCV-SOC of the NMC battery.

(c) OCV versus discharge capacity of the LMO battery.

(d) OCV-SOC of the LMO battery.

Fig. 1. Relationships of OCV versus discharge capacity and OCV-SOC for the NMC (Pozzato et al., 2022) and the LMO batteries (Howey & Birkl, 2017).

The OCV-SOC curve is nearly invariant under aging when the SOC is calculated with the calibrated capacity, as illustrated in Fig. 1. A ρ-near invariance is defined for the calibrated OCV-SOC curve using the average absolute relative error (ARE) between the aged OCV and the nominal OCV as follows.

Definition 1. The OCV-SOC curve is called ρ-near invariant when the average absolute relative error of the OCV on the calibrated OCV-SOC curve compared to the nominal OCV-SOC curve is less than ρ%.

Based on the invariance behavior, a capacity estimation method was developed using OCV-discharge capacity data without relying on prior training or offline OCV tests. The proposed method is developed based on the Stanford aging dataset (Pozzato et al., 2022), which is collected from an NMC battery at a constant temperature of 23 °C. The used dataset covers a capacity loss of up to 8.6%, and the average ARE of the calibrated OCV curves is less than 0.6%. For the result developed based on this dataset, a modeling assumption about the invariance of the OCV-SOC curve used in this method is formulated as follows.

Assumption 1. The OCV-SOC curve $V_{oc}(Z_i^i)$ is assumed ρ-near invariant with $\rho = 0.6$ under aging for the NMC battery in this work at a constant temperature of 23 °C and a capacity loss of less than 8.6%, when the SOC Z_i^i is calculated using the calibrated capacity C_i.

The selection of $\rho = 0.6$ is explained in Section 3.3.

The approximate invariance has been observed in several studies. Pattipati et al. (2014) conducted extensive battery experiments on 34 battery cells of 11 battery chemistries at 8 temperatures and reported that the OCV-SOC curves are nearly identical under different aging and temperature states when the SOC is computed with the calibrated capacity. Kadem (2025) examined data from different datasets of different chemistries and found that the OCV-SOC curve remains nearly constant above 20% SOC when the SOC is normalized by the degraded capacity. When the data are collected with a low-current OCV test, the calibrated OCV-SOC curves remain almost constant across the complete SOC range.

From an electrochemical perspective, the open-circuit potential (OCP) of battery electrodes is determined by their Gibbs free energy of electrode materials (Yao & Viswanathan, 2024). Battery aging often changes the storage capacity of the electrodes rather than affecting the material's electrochemical properties. As a result, the OCP of electrodes is often regarded as invariant during aging (Schmitt et al., 2021). A mechanistic modeling framework reproduces the OCV curve evolution observed in experimental data under dominant degradation modes (Dubarry et al., 2012). Using this framework, the full cell OCV is the difference between the cathode and the anode OCP:

$$V_{oc}(Z_{full}) = V_{cat}(Z_{full}) - V_{an}(Z_{full}), \tag{3}$$

where V_{cat} and V_{an} are the electrode OCPs and Z_{full} is the full cell SOC. Electrode OCPs are determined by the electrode SOCs Z_{cat} and Z_{an} and the shape of relationships $V_{cat}(Z_{cat})$ and $V_{an}(Z_{an})$ are age-invariant. Curves of $V_{cat}(Z_{full})$ and $V_{an}(Z_{full})$ at full cell SOC for the aged cell result from the shifting and scaling of the electrode OCPs on the SOC axis (Schmitt, 2023):

$$Z_{full} = Z_{an} \cdot \alpha_{an} + \beta_{an} \tag{4}$$

$$Z_{full} = (1 - Z_{cat}) \cdot \alpha_{cat} + \beta_{cat}, \tag{5}$$

where $\alpha_{cat}, \alpha_{an}$ are the scaling factors and β_{cat}, β_{an} are the translation factors.

The OCP models are used to describe the aging behavior of the OCV curve due to the loss of lithium inventory (LLI) and the loss of active materials (LAMs) modes. In the LLI mode, the change in the OCP model is a shift of the anode OCP curve along the SOC axis. Because of the specific shape of the anode OCP curve, under moderate aging, normalization by the calibrated capacity on the SOC reverses the OCV shaping due to the anode OCP shifting, resulting in close alignment with the nominal OCV-SOC relationship (Schmitt, 2023). An exemplary pair of OCP curves can be found in Abbasi et al. (2025).

The LLI is reported as the dominant degradation mode for moderate aging with a capacity loss of up to 10% (Karger et al., 2024). To the moderate extent of degradation, the invariance assumption on the calibrated OCV-SOC curve can be adopted more reliably. As the battery approaches severe aging with a capacity loss of more than 10%, the LAMs can emerge, and the assumption of the OCV invariance can be impaired by a larger value of ρ. In this work, an NMC battery with a capacity loss of less than 8.6% at a constant temperature of 23 °C is considered, and the battery dataset is validated to satisfy Assumption 1. The quantification of the boundary for aging, temperature, and the range of chemistries at which Assumption 1 is not fulfilled is a limitation of the current study and requires further investigation.

In addition to the invariance of the OCV relationship, the following assumption is adopted on the data of the OCV-SOC curves obtained from the nominal and aged batteries.

Assumption 2. The OCV $V_{oc}^n(Z_n^n)$ of the nominal battery obtained from the OCV test and the OCV $V_{oc}^a(Z_a^a)$ of the aged battery extracted from the OCV test or dynamic data are strictly monotonic and bijective with respect to SOC.

Assumption 2 is applied to the OCV data obtained from the OCV test for the nominal battery, and the OCV data for the aged battery, obtained through either an OCV test or identification algorithms. In this work, discharge data is used for capacity estimation, and the nominal OCV data is collected from a single discharge low-current OCV test. The monotonically discharged single-path profile prevents hysteresis behavior from affecting the OCV data of the nominal battery. The OCV is strictly monotonically increasing with SOC (Yao & Viswanathan, 2024). In the single-path experiment, the OCV of the nominal battery is then a bijective function of the SOC. For an aged battery, when the OCV is measured via an OCV test, a similar result to the nominal battery's OCV can be obtained, and the OCV curve will be bijective with SOC. When the OCV of the aged battery is obtained from dynamic data using identification algorithms, the OCV can be imposed as monotonically increasing with SOC by adding constraints to the identification problem (Wang & Ferrari, 2025), ensuring the bijectivity in the OCV-SOC relationship. The bijectivity assumption allows for deriving a locally unique solution for capacity estimation.

2.3. Capacity estimation based on OCV invariance

The invariance property is leveraged to estimate the battery's capacity. For the error in the OCV curves of less than $\rho\%$, when the calibrated SOC of the aged and the nominal battery are equal, i.e., $Z_a^a(t) = Z_n^n(t)$, the OCVs of the two batteries at the calibrated SOC are assumed to be equal, i.e., $V_{oc}^a(Z_a^a(t)) := V_{oc}^n(Z_n^n(t))$, and then there is:

$$V_{oc}^a(Z_a^a(t)) := V_{oc}^n(Z_a^a(t)). \tag{6}$$

The influence of the modeling error of $\rho\%$ will be analyzed in Section 3.3. The OCV of the aged battery $V_{oc}^a(t)$ can be obtained from dynamic discharge data using OCV identification algorithms (Wang & Ferrari, 2025). When the OCV $V_{oc}^a(t)$ of the aged battery is obtained, the calibrated SOC $Z_a^a(t)$ can be found from the nominal OCV-SOC relationship $V_{oc}^n(Z_n^n(t))$ by searching for the SOC $Z_n^n(t)$ that provides the same value of OCV $V_{oc}^n(Z_n^n(t))$ as the aged OCV $V_{oc}^a(t)$.

The discharged capacity $Q_{dc}^a(t)$ of the aged battery is computed using (1) and the calibrated SOC $Z_a^a(t)$ is defined with an unknown calibrated capacity C_a and unknown initial SOC $Z_a^a(t_0)$. Then, the aged capacity C_a and the initial SOC $Z_a^a(t_0)$ can be obtained from an optimization problem that minimizes the error between the OCV of the aged battery and the OCV from the nominal OCV-SOC relationship.

Let $C_a \in \mathbb{R}$ be the capacity of the aged battery, $Z_a^a(t_0) \in [0, 1]$ be the initial SOC of $Z_a^a(t)$. Using the definition of SOC (2), the calibrated SOC $Z_a^a(t)$ of the aged battery can be expressed as:

$$Z_a^a(t) = Z_a^a(t_0) - \frac{Q_{dc}^a(t)}{C_a} \times 100\%. \tag{7}$$

By letting the OCV of the nominal OCV-SOC relationship $V_{oc}^n(Z_n^n(t))$ evaluated at the calibrated SOC $Z_a^a(t)$ equal the OCV $V_{oc}^a(t)$ of the aged battery, the calibrated capacity C_a and the initial SOC $Z_a^a(t_0)$ can be estimated by solving the following optimization problem:

$$\min_{C_a, Z_a^a(t_0)} \|V_{oc,m}^a - V_{oc,m}^n(Z_{a,m}^a)\|_F^2 \tag{8}$$

$$\text{s.t. } C_a > 0 \tag{9}$$

$$Z_a^a(t_0) \in [0, 1], \tag{10}$$

where $\|\cdot\|_F$ is the Frobenius norm, $V_{oc,m}^a \in [\check{V}_{oc}^n, \hat{V}_{oc}^n] \subset \mathbb{R}^{m+1}$ is the vector of OCVs of the aged battery $V_{oc}^a(t)$, $\check{V}_{oc}^n, \hat{V}_{oc}^n \in \mathbb{R}, \check{V}_{oc}^n \leq \hat{V}_{oc}^n$ are the lower and upper bounds of the OCV in the nominal relationship $V_{oc,m}^n(Z_{n,m}^n)$, and $V_{oc,m}^n(Z_{a,m}^a) \in \mathbb{R}^{m+1}$ is the vector of OCVs of the OCV-SOC relationship $V_{oc}^n(Z_n^n(t))$ evaluated at $Z_{a,m}^a$:

$$V_{oc,m}^a = \begin{bmatrix} V_{oc}^a(t_0) \\ V_{oc}^a(t_1) \\ \vdots \\ V_{oc}^a(t_m) \end{bmatrix}, \; V_{oc,m}^n(Z_{a,m}^a) = \begin{bmatrix} V_{oc}^n(Z_a^a(t_0)) \\ V_{oc}^n(Z_a^a(t_1)) \\ \vdots \\ V_{oc}^n(Z_a^a(t_m)) \end{bmatrix}. \tag{11}$$

$Z_{a,m}^a \in \mathbb{R}^{m+1}$ is the vector of SOCs written by discharge capacity $Q_{dc}^a(t)$ and initial value $Z_a^a(t_0)$ with (7):

$$Z_{a,m}^a = \mathbf{1} \cdot Z_a^a(t_0) - \frac{1}{C_a} \begin{bmatrix} Q_{dc}^a(t_0) \\ Q_{dc}^a(t_1) \\ \vdots \\ Q_{dc}^a(t_m) \end{bmatrix}, \tag{12}$$

where $\mathbf{1} \in \mathbb{R}^{m+1}$ is a vector of 1, $t_k := kT, k \in \mathbb{Z}_1^m$ is the kth time instant, and $T \in \mathbb{R}_{>0}$ is the sampling time.

The evaluation $V_{oc,m}^n(Z_{a,m}^a)$ of the OCV-SOC relationship $V_{oc}^n(Z_n^n(t))$ at $Z_{a,m}^a$ can be realized from two sequences $V_{oc}^n(t)$ and $Z_n^n(t)$ via linear interpolation. As the nominal OCV-SOC curve is bijective and monotonically increasing, the condition $V_{oc,m}^a \in [\check{V}_{oc}^n, \hat{V}_{oc}^n]$ ensures that the estimated initial SOC is within the range $[\check{Z}_n^n, \hat{Z}_n^n]$ and is a reliable estimate without extrapolation. The constraints in (9) and (10) ensure that the estimated capacity is positive and the initial SOC is within the feasible range $[0, 1]$.

Remark 1. In the optimization problem (8), the parameters $C_a \in \mathbb{R}$ and $Z_a^a(t_0) \in \mathbb{R}$ are transformed into an OCV vector $V_{oc}^n(Z_{a,m}^a) \in \mathbb{R}^{m+1}$ via the SOC Eq. (12) and the nonlinear OCV-SOC relationship $V_{oc}^n(Z_n^n)$ to minimize the cost function. Because of the nonlinearity of $V_{oc}^n(Z_n^n)$, the feasible set $\mathcal{V} \subset \mathbb{R}^{m+1}$ for the candidate $V_{oc}^n(Z_{a,m}^a)$ is non-convex, and thus the optimization problem (8) potentially has multiple minima. The uniqueness of the global minimum depends on the OCV measurement $V_{oc,m}^a$, and the location the optimization converges to varies with initialization. For the OCV $V_{oc,m}^a$ of an aged battery from the data in this work, the RMSE of OCV in (8) is locally convex over a realistic range of parameters, and the minimizer is near the true parameters, as illustrated in Fig. 2. Problem (8) is thus empirically verified to converge to a unique local minimum. The precision of the estimated capacity is influenced by the invariance error ρ of the OCV-SOC curves and is studied in Section 3.3.

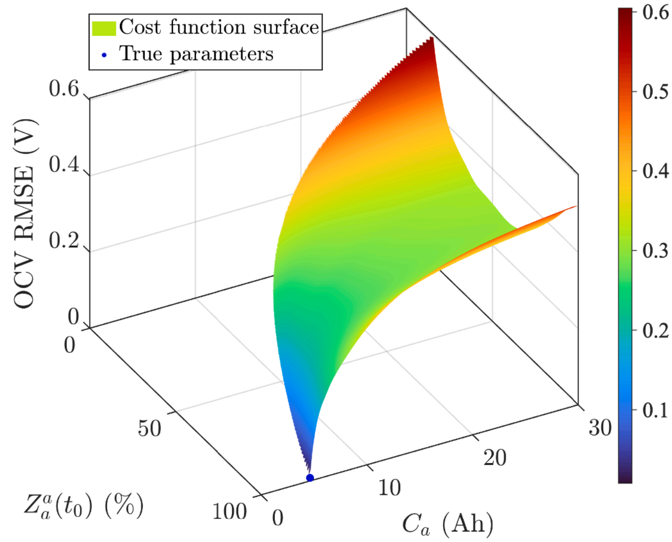

Fig. 2. The surface of the RMSE of OCV in the optimization (8) over the parameters C_a and $Z_a^a(t_0)$ near the true parameters of the aged battery used in this work.

Remark 2. The initial SOC and the aged capacity are mutually dependent. If the two variables were solved for independently and the solution for the initial SOC was inaccurate, the solution for the aged capacity would have needed to compensate for it in order to minimize the overall optimization error. Therefore, both $Z_a^a(t_0)$ and C_a are simultaneously optimized in problem (8) to estimate the aged capacity of the battery.

To validate the fulfillment of invariance with the obtained capacity C_a and initial SOC $Z_a^a(t_0)$, the calibrated OCV-SOC relationship $V_{oc}^a(Z_a^a(t))$ is derived from the discharge capacity $Q_{dc}^a(t)$ and the OCV $V_{oc}^a(t)$, then compare it with the nominal relationship. An uncalibrated SOC with an initial value of one is defined as $\tilde{Z}_n^a(t) := 1 - D_n^a(t)$, where $D_n^a(t) := Q_{dc}^a(t)/C_n$ is the depth of discharge. The calibrated relationship $V_{oc}^a(Z_a^a(t))$ can be obtained from the uncalibrated relationship $V_{oc}^a(\tilde{Z}_n^a(t))$ by applying the following transformation to $\tilde{Z}_n^a(t)$ as:

$$Z_a^a(t) = k\tilde{Z}_n^a(t) + b, \tag{13}$$

where $k := C_n/C_a \in \mathbb{R}$ is the scaling factor and $b := Z_a^a(t_0) - k \in \mathbb{R}$ is the translation factor of the transformation. The transformation can be interpreted as a scaling and translating operation to the SOC axis of the OCV-SOC relationship. It is illustrated by an example shown in Fig. 3. Under the condition that the OCV-SOC relationship is practically invariant and the C_a and $Z_a^a(t_0)$ are accurately identified, the transformed OCV-SOC relationship $V_{oc}^a(Z_a^a(t))$ will align with the nominal relationship $V_{oc}^n(Z_n^n(t))$.

Remark 3. The linear transformation in (13) is a direct consequence of the SOC definition in (2). A nonlinear one could potentially increase the

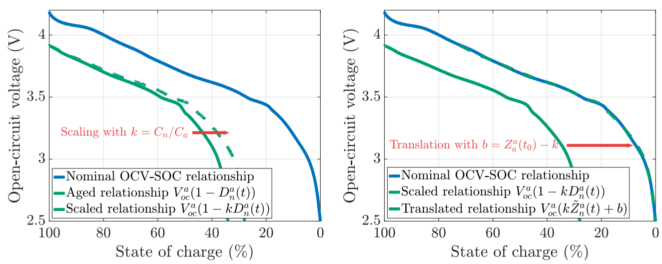

(a) Scaling (b) Translation

Fig. 3. Scaling and translation of the uncalibrated OCV-SOC relationship for capacity estimation.

Table 1
Specifications of the tested battery.

Specification	Value
Battery chemistry	LiNiMnCoO2/Graphite and silicon
Nominal voltage	3.63 V
Nominal capacity	4.85 Ah
Higher cutoff voltage	4.2 V
Lower cutoff voltage	2.5 V

fitting accuracy, but would miss a physical interpretation. It is important to note that such a transformation can be validly applied independently of the fact that the capacity fade may experience a knee point and a faster degradation close to the end of the battery life. Indeed, this would only affect the speed at which the capacity degrades, not its effect on the SOC and, thanks to Assumption 1, its effect on the OCV curve.

Remark 4. As the invariance condition can be satisfied over a partial segment of the OCV-SOC curve, the developed method can also be applied to partial OCV data from the battery to estimate the capacity.

The developed method utilizes the nominal OCV-SOC relationship $V_{oc}^{n}(Z_n^{n}(t))$ and the OCV $V_{oc}^{a}(t)$ and the discharge capacity $Q_{dc}^{a}(t)$ of the aged battery. The nominal relationship is obtained from an OCV test from a nominal battery, and the aged OCV data $V_{oc}^{a}(t)$ can be obtained from dynamic discharge data using an OCV identification algorithm (Wang & Ferrari, 2025; Wang et al., 2025).

The advantages of the developed method are threefold. First, this method requires only one sequence of the OCV-SOC relationship from the nominal battery, without using intensive battery tests. Second, the developed method allows for estimating the capacity from partial discharge data, eliminating the need to fully charge or discharge the battery. Third, by applying it with an OCV identification algorithm, the capacity can be estimated from dynamic discharge data without using additional battery experiments during maintenance.

In the following section, the capacity estimation method is validated using both OCV test data and dynamic discharge data.

3. Simulation experiments

The effectiveness of the developed method is evaluated for capacity estimation on the Stanford Accelerated Aging dataset (Pozzato et al., 2022). The dataset consists of data from 10 battery cells; each cell underwent intensive aging cycles with a dynamic Urban Dynamometer Driving Schedule (UDDS) profile. This profile is used to simulate real-world driving conditions of electric vehicles. The specifications of the tested batteries are tabulated in Table 1.

In the cycling test, the battery cells were discharged from 80% to 20% SOC and charged using a constant current and constant voltage profile. After certain aging cycles, an offline low-current OCV test was performed to measure the battery's OCV and capacity. The number of aging cycles experienced by each battery cell before a selection from

Table 2
Number of aging cycles undergone by battery cells before a selection of OCV test cycles.

Cell label	Number of aging cycles before the OCV test							
	1	3	5	7	9	11	13	15
W3	0	75	–	–	–	–	–	–
W4	0	75	132	176	–	–	–	–
W5	0	75	159	187	219	269	319	369
W7	0	75	141	–	–	–	–	–
W8	0	75	148	151	185	247	297	347
W9	0	75	144	146	179	241	291	341
W10	0	75	146	151	188	250	300	350
G1	0	30	62	112	162	212	–	–
V4	0	45	95	145	194	244	–	–
V5	0	18	–	–	–	–	–	–

15 OCV test rounds is tabulated in Table 2. The first test was conducted before the aging cycles began, and the OCV and SOC data collected from the first test are used as the nominal OCV-SOC relationship for validation of capacity estimation. A total of 15 OCV tests were performed during the aging campaign, and some battery tests were terminated earlier; these tests are denoted by "-" in the table.

3.1. *Capacity estimation from OCV test data*

In this subsection, the capacity estimation method is validated using the OCV test data in the accelerated aging dataset. The cells' OCVs and discharge capacities were collected from each OCV test, then these data and the nominal OCV-SOC relationship from the first OCV test were used to estimate the battery's capacity. The estimation was conducted on each OCV test cycle, and the estimated results were compared with the measured capacities from the corresponding OCV test. The calibrated capacity C_a and the initial SOC $Z_a^{a}(t_0)$ are estimated by solving (8). The capacity estimation performance is evaluated using the Absolute Relative Error (ARE) defined as:

$$\mathrm{ARE} = \frac{|\overline{C}_a - C_a|}{|C_a|} \times 100\%, \tag{14}$$

where $\overline{C}_a \in \mathbb{R}$ is the estimated capacity and $C_a \in \mathbb{R}$ is the actual capacity of the aged battery measured at the OCV test.

The capacity at each round of the OCV test was estimated for every cell in the dataset. The results are grouped by cell to validate the statistical robustness of the estimation across OCV test cycles. The AREs of capacity estimation of battery cells are illustrated in the box plot in Fig. 4. The median errors are shown by the middle bars, and the upper and lower boundaries of the boxes are the 75% and 25% percentiles. Fig. 4 shows that the AREs of the estimates are mostly less than 1% across cells, and the median ARE is all less than 0.5%. A noticeably small error is found for cell W3, and the two highest errors are identified for cell W7 and V5. Since cell W3 has only 2 samples and cells W7 and V5 have only 3 sample points, reported in Table A.7, the results on these cells are considered less significant. These results are retained for completeness of the validation.

Out of 10 battery cells, the maximum AREs of 7 cells are below 0.5%. The median ARE for most cells is below 0.3%, and the average AREs of all cells are less than 0.4%. The sufficient accuracy in capacity estimation across 10 cells demonstrates the robustness of the developed method based on the OCV-SOC relationship (numerical values are provided in Table A.7 in the appendix).

A representative cell with the largest number of aging cycles, W5, was selected to demonstrate details of capacity estimation over the long aging process as well as to illustrate the transformations in the OCV-SOC relationship for capacity estimation.

Results from OCV test rounds 3, 7, 11, and 15, after the cell underwent 75, 187, 269, and 369 aging cycles, respectively, are shown. The estimated capacities, actual capacities, and estimation AREs at the OCV

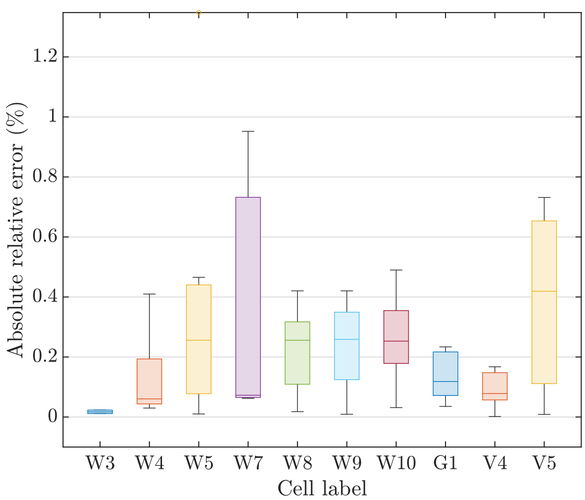

Fig. 4. Box plot of AREs (%) of capacity estimation for each battery cell across all OCV test cycles (the middle bar represents the median value, the upper and lower boundaries of the box are 75% and 25% percentiles, and the upper and lower bars beyond the box cover all data except outliers).

Table 3
Estimated capacities (Ah) and AREs (%) of capacity estimation of cell W5 using OCV test data.

Aging cycle	Estimated capacity (Ah)	Actual capacity (Ah)	ARE (%)
75	4.78	4.78	0.07
187	4.58	4.57	0.11
269	4.53	4.52	0.32
369	4.47	4.45	0.45

test rounds are tabulated in Table 3. It can be seen from the table that the estimated capacities closely align with the actual capacities across all 4 test rounds and exhibit AREs of less than 0.5%.

The OCV-SOC transformations for capacity estimation for the 4 test cycles are illustrated in Fig. 5. The figure shows that the calibrated OCV-SOC curves closely align with the nominal OCV curve, satisfying the practical invariance property of the OCV-SOC relationship. This result indicates the effectiveness of using the invariance relationship in OCV-SOC curves for capacity estimation.

The estimation results on 10 battery cells across 15 test rounds, and the satisfaction of OCV-SOC invariance in capacity estimation, demonstrate the robustness and efficacy of the developed method for capacity estimation using battery's OCV data.

3.2. Capacity estimation from partial OCV test data

The validation of the capacity estimation for partial OCV data was conducted for each cell across all OCV test cycles. For each cycle, 33% of the OCV data from the beginning, middle, and end were used to estimate the capacity. The truncated OCV data with the full nominal OCV-SOC data were used to estimate capacity by solving the optimization problem (8).

Fig. 6 depicts the box plots of estimation AREs of each cell for the three segments across all test cycles. It can be seen from the figure that the aged capacities were effectively estimated with a small estimation ARE. The AREs of using the beginning and last parts of the OCV data are mostly less than 8%, and the AREs of using the middle data exhibit a lower error, mostly less than 4%. The reason for the performance difference is that the middle region of the OCV-SOC curve exhibits greater invariance to the nominal OCV relationship than the beginning and end parts of the OCV data. This is due to the milder nonlinearity in the OCV curve in the middle SOC region. The error of using partial OCV data increased, compared to that with complete OCV data, indicating that incorporating a wider range of OCV for capacity estimation improves estimation accuracy.

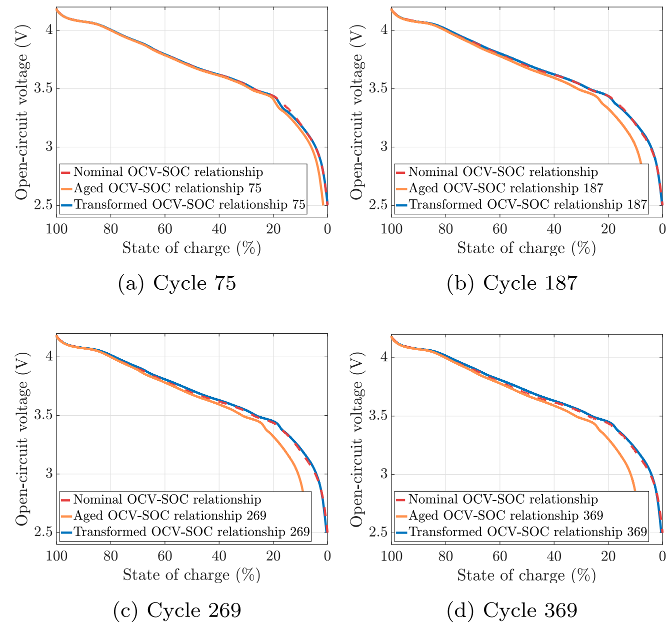

Fig. 5. OCV-SOC transformations of capacity estimation for cell W5 on validation cycles using OCV test data.

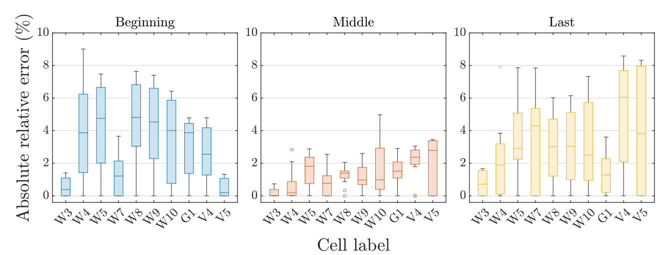

Fig. 6. AREs of capacity estimation across cells and test cycles using the beginning, middle, and last 33% of the OCV data.

Table 4
Estimated capacities (Ah) for cell W5 and W10 using the beginning, middle, and last 33% of the OCV data.

Cell	Cycle	Begin.	Middle	Last	Avg.	Act.
W5	159	4.75	4.58	4.74	4.69	4.63
W5	369	4.78	4.57	4.17	4.51	4.45
W10	146	4.70	4.41	4.93	4.68	4.65
W10	350	4.73	4.40	4.34	4.49	4.46

The results on two exemplary cells, W5 and W10, which have the largest number of aging cycles, are shown to illustrate the estimated capacities and the transformation of the partial OCV-SOC relationship. The validation was conducted on cell W5 after 159 and 369 cycles, and on cell W10 after 146 and 350 cycles. The estimated capacities of the battery cells are shown in Table 4. The average estimated capacities of the two cells closely agree with the actual values, with average AREs of less than 5.5% (numerical values are provided in Table A.8 in the appendix).

The OCV-SOC transformations of cell W5 and W10 using three parts of the OCV data after the two aging cycles are illustrated in Figs. 7 and 8, respectively. The figure shows that transformations using partial OCV data from the beginning, middle, and last parts of the OCV cycles

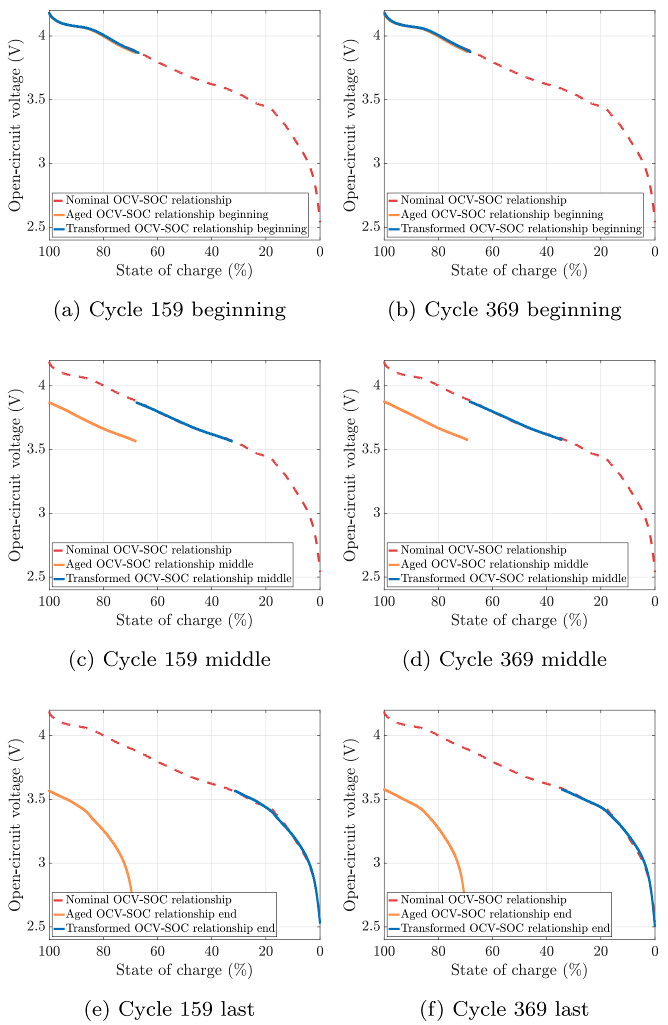

Fig. 7. OCV-SOC transformations of capacity estimation using partial OCV test data of cell W5. (a)(c)(e): transformation after 159 aging cycles. (b)(d)(f): transformation after 369 aging cycles.

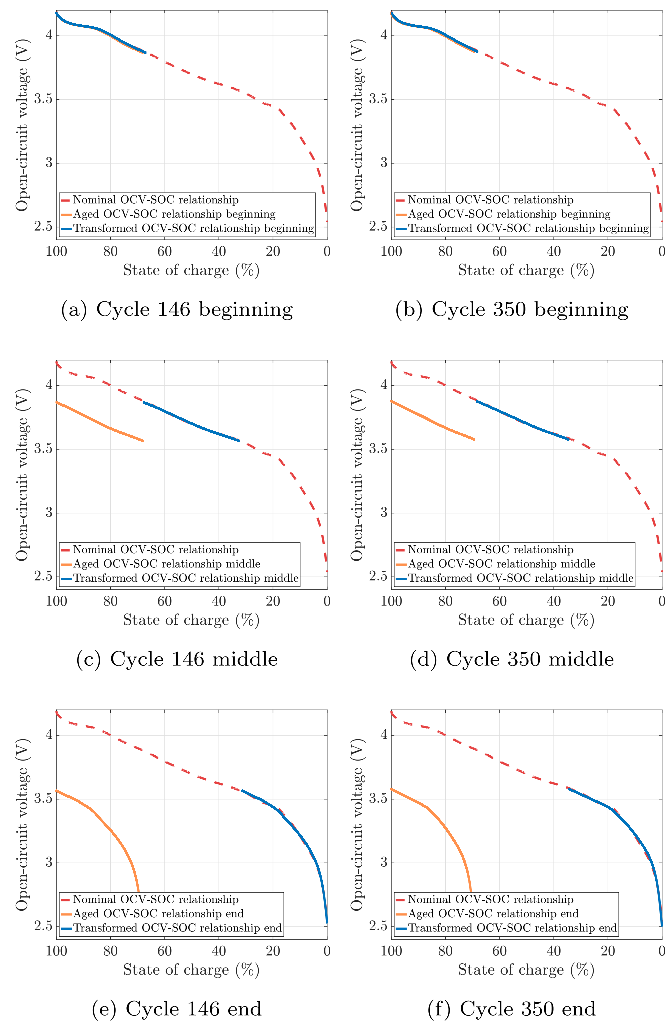

Fig. 8. OCV-SOC transformations of capacity estimation using partial OCV test data of cell W10. (a)(c)(e): transformation after 146 aging cycles. (b)(d)(f): transformation after 350 aging cycles.

all achieve good alignment with the nominal relationships across two cycles in the two cells.

The simulation results using partial OCV data demonstrate the effectiveness and robustness of the developed method for capacity estimation of aged batteries using the practical invariance of the OCV-SOC relationship.

3.3. Influence of OCV invariance on capacity estimation

The influence of the degree of the OCV invariance between the calibrated nominal and aged OCV-SOC relationships on the accuracy of capacity estimation was studied in this section. First, the influence of the range of SOC covered by the data on the estimation performance of the developed method was analyzed. The analysis was conducted using a sliding-window method. The sliding window moves along the calibrated SOC axis from 0% to 100% and collects OCV-discharge capacity data to estimate the aged cell's capacity. The window length varied from 1% to 100% SOC, with the 100% length indicating a single window covering the full discharge cycle data, and the window step size is 1% SOC. The operation was performed on all OCV test data from 4 cells of the largest aging cycles: W5, W8, W9, and W10. Data from 56 test cycles (14 per cell) was collected and the average AREs of estimated capacities across the cycles for each window length were computed. The capacity ARE over the window length is depicted in Fig. 9. The figure shows that the ARE decreases monotonically with increasing window length; a steeper drop is observed at the small and large ends of the window length, and a moderate decrease is shown in the middle SOC range. The result indicates that for a window length less than 3%, the data coverage is insufficiently large to reveal the OCV variation of the entire OCV curve, and adding window length significantly reduces the estimation error. Increasing the window length allows for matching the nominal and aged OCV curves over a wider range. With a SOC range above 80%, the error in locations where the OCV deviation is more significant is averaged, and a more reliable estimation results.

To analyze the effect of the SOC location on the estimation performance, the smallest window length before the ARE curve flattens was selected, which is 3% SOC at the knee point of the curve shown by the circle in Fig. 9, to conduct the sliding window analysis. The average ARE across 56 tests for each window was computed. The median SOC of the window was used to denote the window location. The capacity ARE versus SOC curve is depicted in Fig. 10. The figure shows that the capacity ARE increases at around 20%, 40%, 60%, and 90% SOC. To study the reason for the increased estimation ARE, the derivative of OCV with respect to calibrated SOC (dOCV/dSOC) for the aged and nominal OCV-SOC curves, and the ARE between the two derivatives was computed. The derivative AREs over the calibrated SOCs are depicted in Fig. 10. The figure indicates that the capacity

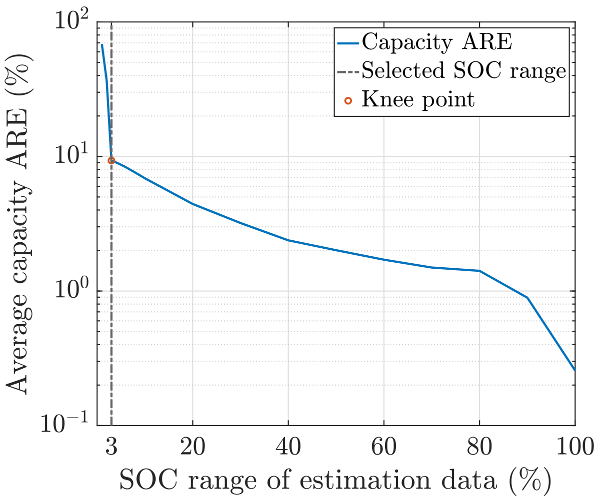

Fig. 9. Average capacity ARE of 56 OCV test data from cells W5, W8, W9, and W10 in relation to the SOC range of capacity estimation data computed using a sliding window with a window length ranging from 1% to 100% SOC.

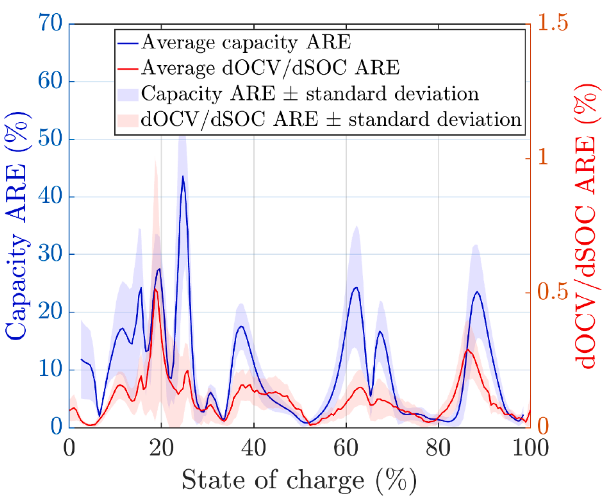

Fig. 10. Capacity estimation ARE and dOCV/dSOC ARE in relation to the calibrated SOC on 56 OCV test data from cells W5, W8, W9, and W10. The correlation coefficient of the two average curves is 0.64.

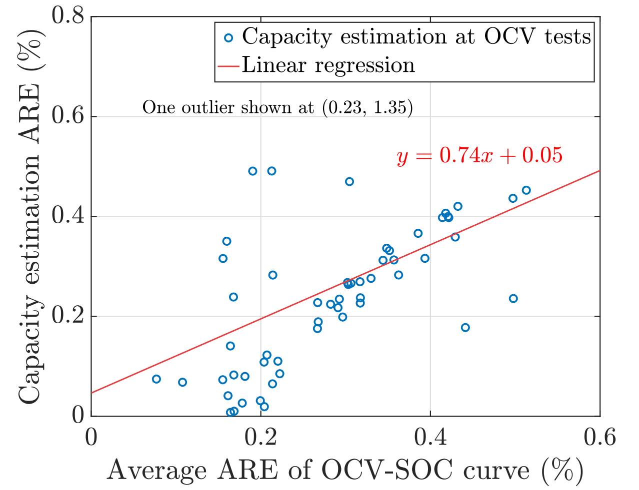

Fig. 11. Capacity estimation ARE in relation to the OCV curve ARE over 56 OCV test data from cells W5, W8, W9, and W10.

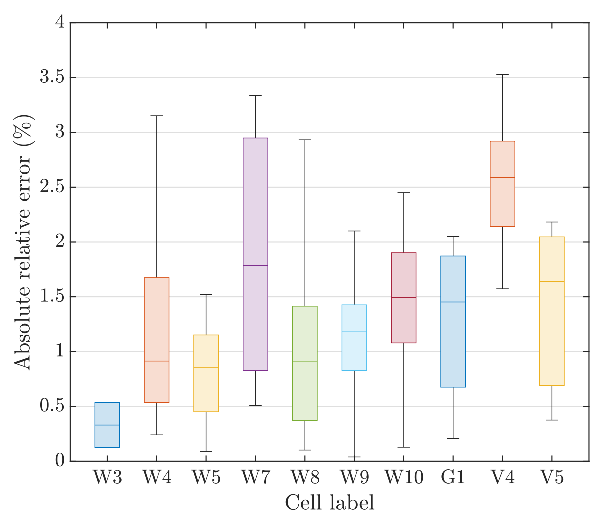

Fig. 12. Box plot of AREs of capacity estimation of each cell using OCV data identified from dynamic discharge data.

ARE is correlated with the dOCV/dSOC ARE. The correlation coefficient is 0.64, indicating a moderately high alignment. The correlation exists because the capacity is estimated by matching the slope $1/C_a$ of the aged OCV-SOC curves in (12) to that of the nominal OCV curve; a larger error in dOCV/dSOC results in a greater distortion of the transformed OCV curve on the SOC axis, leading to a larger error in capacity estimation.

The capacity AREs of a 100% SOC window for all 56 OCV tests, and the average ARE of OCV between the aged and the nominal OCV-SOC curves over the SOC axis were computed. The AREs of estimated capacities in relation to the AREs of the OCV curves of each test are illustrated in Fig. 11. The figure shows that the capacity ARE is positively related to the OCV ARE; a linear equation can be fit with the expression: $y = 0.74x + 0.05$. This result shows that when the OCV ARE is below 0.6%, the capacity estimation error is relatively small, indicating satisfactory performance. The results support the selection of $\rho = 0.6$ as a practical value for near invariance of the OCV curve in capacity estimation.

3.4. *Capacity estimation from dynamic discharge data*

The efficacy of estimating capacities using OCVs identified from dynamic discharge data was validated. The OCV data were identified with an identification algorithm developed in Wang and Ferrari (2025). Dynamic data from the first cycle after each OCV test were used to identify the OCV, and the obtained OCV values were then used to estimate the capacities. The estimated capacities were compared with the capacities measured from the most recent OCV test.

The AREs of capacity estimation for every cell across all OCV test cycles are depicted in the box plot in Fig. 12. The figure shows that all capacity estimation AREs are below 4%, with the median values of 9 battery cells being less than 2%. The maximum ARE for all cells is less than 3.5%, and the average AREs are less than 2% for 9 cells (numerical values are provided in Table A.9 in the appendix). The satisfactory accuracy across multiple test cycles and different cells demonstrates the effectiveness of the developed method for capacity estimation with OCV identified from dynamic discharge data.

The estimated capacities, actual capacities, and the AREs of capacity estimation for cell W5, W10, and V4 at the first and the last estimation cycle are tabulated in Table 5. The results showed that the estimated

Table 5
Estimated capacities (Ah) and estimation ARE (%) using identified OCV-SOC relationships for cell W5, W10, and V4 at the first and the last estimation cycle.

Cell	Cycle	Estimated capacity (Ah)	Actual capacity (Ah)	ARE (%)
W5	0	4.93	4.86	1.52
W5	344	4.51	4.47	0.84
W10	0	4.87	4.87	0.13
W10	325	4.52	4.48	1.03
V4	0	4.76	4.87	2.14
V4	219	4.52	4.62	2.01

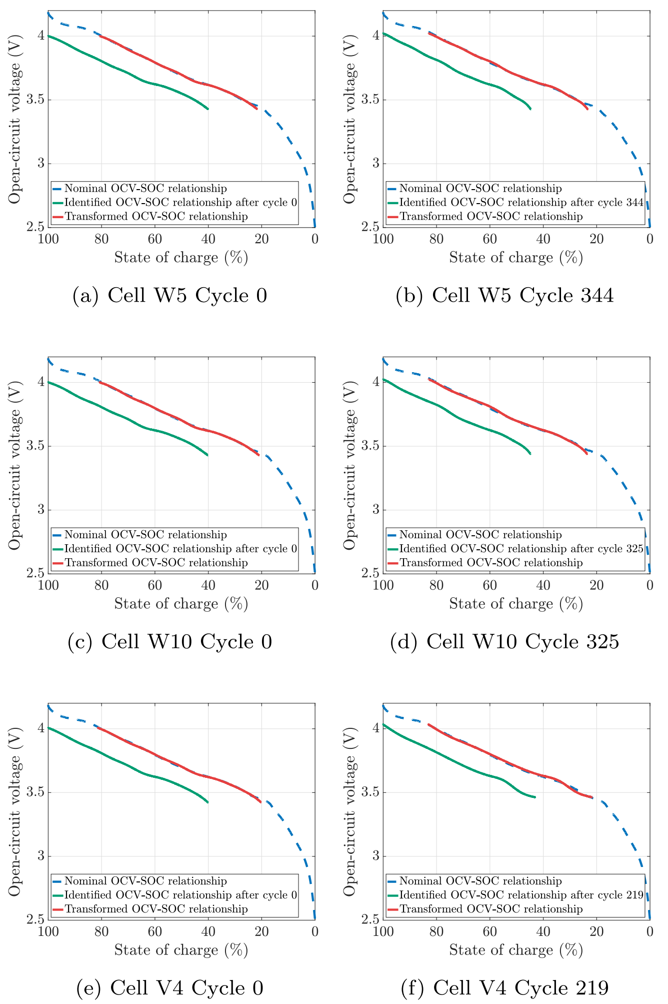

Fig. 13. Transformation of OCV-SOC relationships identified from dynamic discharge data. (a)(b): cell W5 after cycle 0 and 344. (c)(d): cell W10 after cycle 0 and 325. (e)(f): cell V4 after cycle 0 and 219.

capacities exhibit satisfactory agreement with the actual capacities in both the first and last estimation cycles for the three cells.

The identified OCV, actual OCV, and transformed OCV-SOC relationships for cells W5, W10, and V4 at the first and the last estimation cycle are depicted in Fig. 13. The figures illustrate that the OCV curves are effectively identified from the dynamic data for these battery cells, and the transformed OCV-SOC relationships align with the nominal relationships with satisfactory accuracy. The accurate estimation demonstrates the feasibility of using the developed method to estimate battery capacity directly from dynamic operating data without relying on additional OCV tests.

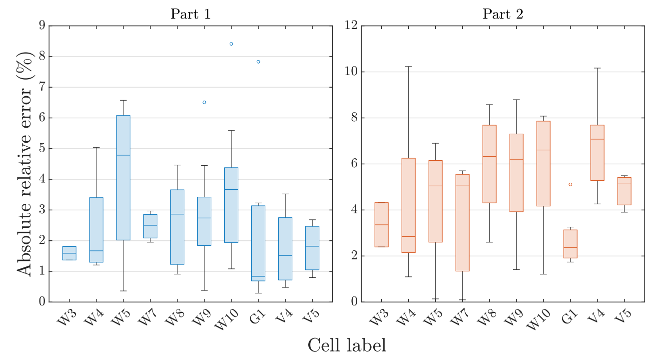

Fig. 14. Box plot of AREs (%) of capacity estimation from dynamic discharge data for each battery cell across the first cycle after OCV tests. Part 1 covers dynamic data from 80% to 50% SOC, and Part 2 covers data from 50% to 20% SOC.

To validate the efficacy of using partial dynamic discharge data to estimate the battery's capacity, the dynamic data is split into two parts. Part 1 covers the data from 80% to 50% of SOC, and Part 2 covers the data from 50% to 20% of SOC. The SOC values were not provided to the capacity estimation algorithm; only discharge capacity was computed, and it was computed anew for each part of the dynamic data. The OCV data were identified for each part of the dynamic data, and the identified OCVs were used to estimate the battery's capacity. The validations were conducted for every cell across the first dynamic data after each OCV test. The AREs of capacity estimation for each cell are depicted in Fig. 14. The figure shows that cell capacities were effectively estimated from partial discharge data. The AREs of part 1 are mostly below 6%, and those of part 2 are mainly below 8%. This is sufficient accuracy, given that the partial data were derived from dynamic discharge data and cover only 30% of SOC.

Results from partial dynamic discharge data demonstrate the robustness of the developed method for capacity estimation. The results present potential for efficient capacity estimation using only dynamic discharge data.

3.5. Comparison with different estimation methods

In this section, the developed approach is compared with the modified-linear model method (Sivalertporn et al., 2025) and the equivalent circuit model (ECM) method (Li et al., 2024) for capacity estimation. The comparison was conducted on cells W5, W8, W9, and W10, which have the highest cycle counts.

The modified linear model was trained on the cell's capacity-cycle data before cycle 80 and used to estimate the remaining capacity. The ECM was first identified from dynamic data across full aging cycles, and then a 6th-order polynomial was fitted to relate the identified parameters to the cell's capacity. A leave-one-out scheme was used for capacity estimation, in which the model was trained on three other cells and validated on the 4th test cell. The capacities over aging cycles estimated by the three methods, compared with the actual capacities, are illustrated in Fig. 15. The figure shows that the developed method effectively captures the trend in the degraded capacities of the four cells, with higher accuracy for cells W5, W8, and W9 and lower accuracy for cell W10. The increased error in cell W10 may be attributed to cell-specific identification errors in the OCV curve, which may affect the scaling of the aged OCV to accurately match the nominal OCV curve.

The average AREs across 4 cells of the three estimation methods are tabulated in Table 6. The table shows that the ECM method has an ARE of 0.9%, the developed method has an average ARE of 1.1%, and the modified linear model method results in an average ARE of 1.3%. The developed method presents higher accuracy than the modified-linear model, while lower than the ECM method. The ECM method

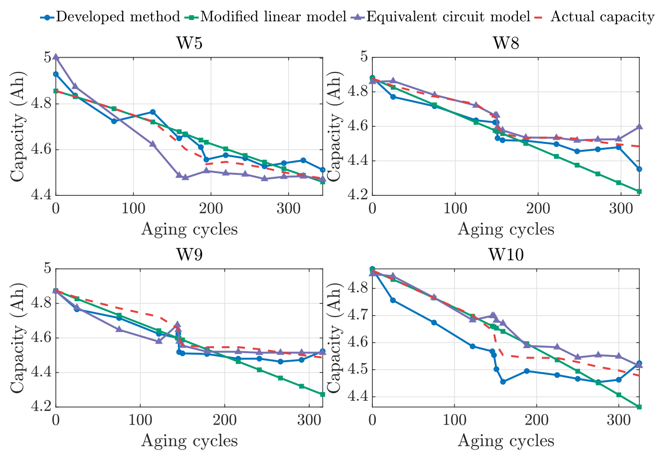

Fig. 15. Capacity estimation of the developed method, the modified-linear model, and the equivalent circuit model method.

Table 6
Average ARE (%) of capacity estimation by the three estimation algorithms on cell W5, W8, W9, and W10.

Cell	Developed method	Modified-linear model	Equivalent circuit model
W5	0.82	0.69	1.35
W8	1.07	2.04	0.45
W9	1.09	1.6	0.75
W10	1.46	0.87	0.94
Average	1.11	1.3	0.87

involves training on 3 cells over full aging cycles to learn capacity curves, which is more data-intensive than the developed method. The modified-linear model requires OCV obtained from offline tests for model training and is subject to extrapolation error, as shown on cells W8 and W9 in Fig. 15. The developed method estimates capacities from dynamic discharge data without requiring additional training or offline OCV tests, achieving high data efficiency while maintaining satisfactory accuracy.

The comparison study demonstrates the accuracy and the high efficiency of the developed approach for capacity estimation using dynamic data without requiring extensive model training or prolonged offline OCV tests. The experimental results illustrate the efficacy of the developed method in estimating the capacity of aged batteries using full OCV, partial OCV, and OCV identified from dynamic discharge data. The developed method achieves performance comparable to that of training-based methods while exhibiting higher efficiency without relying on intensive battery testing.

4. Discussion

This study presents a novel method for capacity estimation that uses the battery's dynamic discharge data, without relying on an intensive battery OCV test. Estimation results across OCV test data, partial OCV data, and dynamic discharge data from 10 cells validate the efficacy and robustness of the developed method for capacity estimation. The effectiveness and accuracy are attributed to the practical invariance in the OCV-SOC relationship recorded from multiple battery cells, datasets, and validated across different studies (Kadem, 2025; Pattipati et al., 2014). Compared to other model-based and empirical approaches, this method does not rely on a training dataset and avoids parameter pre-tuning, presenting high data efficiency and implementation stability.

The results in this work are obtained at a fixed temperature. Several studies revealed a nearly invariant OCV-SOC relationship across different temperatures when the SOC is computed with the calibrated capacity (Kadem, 2025; Pattipati et al., 2014). Therefore, it is hypothesized that the developed method will perform effectively under variable-temperature conditions. However, the actual validation and performance of the developed method under varying temperature conditions still need further investigation. In this paper, the developed method has been validated on laboratory data. The method's performance on real-world battery data from operational electric vehicles requires further investigation.

5. Conclusion

In this work, a capacity estimate method was developed based on the discharge capacity and the nominal OCV-SOC relationship. The estimation is achieved through an invariance property in the OCV-SOC relationship across aging cycles. With the invariance, the capacity can be estimated by solving an OCV alignment optimization problem using the OCV of the aged battery. This approach applies to partial OCV data without using a full cycle of battery operation. With an OCV identification algorithm, the capacity can be estimated from dynamic discharge data. Simulation experiments showed an average ARE of less than 0.4% with OCV test data and less than 2.6% with dynamic discharge data across 10 battery cells for capacity estimation, demonstrating accuracy that is effective for practical use in EV batteries. In future work, the developed approach will be extended to predict the remaining useful life of the battery.

CRediT authorship contribution statement

Yang Wang: Writing – original draft, Visualization, Validation, Software, Methodology, Investigation, Formal analysis, Conceptualization; **Marta Zagorowska:** Writing – review & editing, Supervision; **Riccardo M.G. Ferrari:** Writing – review & editing, Supervision, Resources, Project administration, Funding acquisition.

Declaration of competing interest

The authors declare that they have no known competing financial interests or personal relationships that could have appeared to influence the work reported in this paper.

Acknowledgment

This research has been funded by Volvo AB (Sweden) and NWO (Netherlands) (Grant No. TKI-HTSM 21.0056). M. Zagorowska also kindly acknowledges the funding from the Delft Technology Fellowship.

Appendix A. Statistics of AREs (%) in capacity estimation of battery cell

Table A.7
AREs (%) of capacity estimation of battery cells using OCV test data.

Cell label	Min ARE	Max ARE	Median ARE	Average ARE	Estimation samples
W3	0.011	0.023	0.017	0.017	2
W4	0.030	0.410	0.061	0.132	7
W5	0.010	1.348	0.256	0.317	14
W7	0.062	0.952	0.073	0.362	3
W8	0.018	0.420	0.256	0.236	14
W9	0.009	0.420	0.259	0.243	14
W10	0.031	0.490	0.253	0.259	14
G1	0.035	0.234	0.118	0.133	10
V4	0.002	0.167	0.078	0.093	10
V5	0.009	0.732	0.419	0.387	3

Table A.8
AREs (%) of capacity estimation for cell W5 and W10 using the beginning, middle, and last 33% of the OCV data.

Cell	Cycle	Beginning	Middle	Last	Average
W5 - min	159	2.6949	1.0627	2.4023	2.0533
W5 - max	369	7.4267	2.6346	6.3283	5.4632
W10 - min	146	1.2709	4.9790	6.1052	4.1184
W10 - max	350	6.0340	1.2623	2.5761	3.2908

Table A.9
AREs (%) of capacity estimation of battery cells using OCV identified from dynamic discharge data.

Cell label	Min ARE	Max ARE	Median ARE	Average ARE	Estimation counts
W3	0.124	0.535	0.330	0.330	2
W4	0.240	3.152	0.913	1.224	7
W5	0.090	1.520	0.857	0.817	14
W7	0.508	3.337	1.785	1.877	3
W8	0.102	2.932	0.913	1.065	14
W9	0.039	2.100	1.180	1.092	14
W10	0.127	2.450	1.495	1.463	14
G1	0.208	2.049	1.453	1.296	10
V4	1.573	3.529	2.588	2.549	10
V5	0.375	2.182	1.639	1.399	3

References

Abbasi, A., Gharehghani, A., & Andwari, A. (2025). Real-time discharge curve and state of charge estimation of lithium-ion batteries via a physics-informed full homogenized macroscale model. *Journal of Energy Storage*, *135*, 118307.
Bloom, I., Jansen, A. N., Abraham, D. P., Knuth, J., Jones, S. A., Battaglia, V. S., & Henriksen, G. L. (2005). Differential voltage analyses of high-power, lithium-ion cells: 1. Technique and application. *Journal of Power Sources*, *139*(1-2), 295–303.
Dubarry, M., Truchot, C., & Liaw, B. Y. (2012). Synthesize battery degradation modes via a diagnostic and prognostic model. *Journal of Power Sources*, *219*, 204–216.
El-Dalahmeh, M., Al-Greer, M., El-Dalahmeh, M., & Bashir, I. (2023). Physics-based model informed smooth particle filter for remaining useful life prediction of lithium-ion battery. *Measurement*, *214*, 112838.
Hannan, M. A., Lipu, M. S. H., Hussain, A., & Mohamed, A. (2017). A review of lithium-ion battery state of charge estimation and management system in electric vehicle applications: Challenges and recommendations. *Renewable and Sustainable Energy Reviews*, *78*, 834–854.
Howey, D., & Birkl, C. (2017). In *Oxford battery degradation dataset 1 Data repository: Oxford University Research Archive (ORA) ed.1*, University of Oxford Data collected https://ora.ox.ac.uk/objects/uuid:03ba4b01-cfed-46d3-9b1a-7d4a7bdf6fac
Kadem, O. (2025). Co-estimation of state of health and state of charge for lithium-ion batteries via the normalized state of charge and open circuit voltage relationship. *Energy Storage*, *7*(7), e70270.
Karger, A., Schmitt, J., Kirst, C., Singer, J. P., Wildfeuer, L., & Jossen, A. (2024). Mechanistic cycle aging model for the open-circuit voltage curve of lithium-ion batteries. *Journal of Power Sources*, *593*, 233947.
Li, Y., Wang, L., Feng, Y., Liao, C., & Yang, J. (2024). An online state-of-health estimation method for lithium-ion battery based on linear parameter-varying modeling framework. *Energy*, *298*, 131277.
Lianpo, L., Songmei, D., & Lin, W. (2025). Capacity degradation prediction of electric vehicle battery by integrating convolutional neural network with informer model. *Journal of Power Sources*, *651*, 237497.
Lu, J., Xiong, R., Tian, J., Wang, C., Hsu, C.-W., Tsou, N.-T., Sun, F., & Li, J. (2022). Battery degradation prediction against uncertain future conditions with recurrent neural network enabled deep learning. *Energy Storage Materials*, *50*, 139–151.
Meng, J., Luo, G., Ricco, M., Swierczynski, M., Stroe, D.-I., & Teodorescu, R. (2018). Overview of lithium-ion battery modeling methods for state-of-charge estimation in electrical vehicles. *Applied Sciences*, *8*(5), 659.
Navidi, S., Thelen, A., Li, T., & Hu, C. (2024). Physics-informed machine learning for battery degradation diagnostics: A comparison of state-of-the-art methods. *Energy Storage Materials*, *68*, 103343.
Pattipati, B., Balasingam, B., Avvari, G. V., Pattipati, K. R., & Bar-Shalom, Y. (2014). Open circuit voltage characterization of lithium-ion batteries. *Journal of Power Sources*, *269*, 317–333.
Peng, S., Wang, Y., Tang, A., Jiang, Y., Kan, J., & Pecht, M. (2025). State of health estimation joint improved grey wolf optimization algorithm and LSTM using partial discharging health features for lithium-ion batteries. *Energy*, *315*, 134293.
Plett, G. L. (2015). Battery management systems, Volume I: Battery modeling (vol. 1). Artech House.
Pozzato, G., Allam, A., & Onori, S. (2022). Lithium-ion battery aging dataset based on electric vehicle real-driving profiles. *Data in Brief*, *41*, 107995.
Schmitt, J. (2023). State of health estimation for lithium-ion batteries. Ph.D. thesis. Technische Universität München.
Schmitt, J., Rehm, M., Karger, A., & Jossen, A. (2023). Capacity and degradation mode estimation for lithium-ion batteries based on partial charging curves at different current rates. *Journal of Energy Storage*, *59*, 106517.
Schmitt, J., Schindler, M., & Jossen, A. (2021). Change in the half-cell open-circuit potential curves of silicon–graphite and nickel-rich lithium nickel manganese cobalt oxide during cycle aging. *Journal of Power Sources*, *506*, 230240.
Sivalertporn, K., Poopanya, P., & Phophongviwat, T. (2025). Capacity forecasting of lithium-ion batteries using empirical models: Toward efficient SOH estimation with limited cycle data. *Energies*, *18*(14), 3828.
Wan, Z., Pannala, S., Solbrig, C., Garrick, T. R., Stefanopoulou, A. G., & Siegel, J. B. (2025). Degradation and expansion of lithium-ion batteries with silicon/graphite anodes: Impact of pretension, temperature, c-rate and state-of-charge window. *eTransportation*, *24*, 100416.
Wang, Y., & Ferrari, R. M. G. (2025). Direct continuous-time LPV system identification of li-ion batteries via l1-regularized least squares. In *2025 IEEE 64th Conference on decision and control (CDC)* (pp. 2347–2352). IEEE.
Wang, Y., Ferrari, R. M. G., & Verhaegen, M. (2025). Continuous-time system identification and OCV reconstruction of Li-ion batteries via regularized least squares. In *2025 European control conference (ECC)* (pp. 2291–2296). IEEE.
Wang, Z., Zhao, X., Fu, L., Zhen, D., Gu, F., & Ball, A. D. (2023). A review on rapid state of health estimation of lithium-ion batteries in electric vehicles. *Sustainable Energy Technologies and Assessments*, *60*, 103457.
Yao, A. M., & Viswanathan, V. (2024). Open-circuit voltage models should be thermodynamically consistent. *The Journal of Physical Chemistry Letters*, *15*(4), 1143–1151.
Zagorowska, M., Wu, O., Ottewill, J. R., Reble, M., & Thornhill, N. F. (2020). A survey of models of degradation for control applications. *Annual Reviews in Control*, *50*, 150–173.
Zhang, K., Lv, T., Chen, X., Chen, J., Shen, Y., Zhou, L., Sun, T., & Zheng, Y. (2025). Study on battery capacity recognition method for real electric vehicle under complex operating conditions. *Journal of Energy Storage*, *118*, 116219.